

ULTRA-HIGH RESOLUTION VISUALIZATION OF GROUND DEFORMATION AND STRUCTURAL FAILURE USING GROUND-LIDAR: EXAMPLES FROM THE NIIGATA KEN CHUETSU EARTHQUAKE

Robert KAYEN¹, Brian COLLINS², Peter DARTNELL¹, Gerald BAWDEN³,
Scott ASHFORD⁴, Nicholas SITAR²

¹U.S. Geological Survey, Menlo Park, CA

²University of California at Berkeley, Berkeley, CA

³U.S. Geological Survey, Sacramento, CA

⁴University of California at San Diego, La Jolla, CA

SUMMARY

Natural and man-made disasters leave in their wake deformed ground and structures. Deformations can take on extremely complex surfaces and shapes that are beyond the ability of post-event investigators to accurately measure or visualize for analysis using conventional survey methods. A new technology, 3-D laser-scanning Light Detection And Ranging (LIDAR), allows for rapid and remote sensing of damaged terrain. Scanning LIDAR targets the damaged area with sequenced LASER pulses from which distance and orientation are computed. A digital terrain model of the damaged region is constructed by sweeping the laser-scanner across the target area in controlled steps and accounting for the 3-dimensional position of the reflected target. Two forms of LIDAR surveys, airborne and ground, are available for post-disaster characterization of deformations, though airborne LIDAR is primarily useful for regional-scale assessment of the damage region, with a target-area footprint of several square meters and a position error of 15-20 cm. Ground-based LIDAR has an accuracy range of 0.5-2.5 cm, about an order of magnitude greater than airborne LIDAR systems, and a target-area footprint as low as sub-cm. During a single tripod-mounted LIDAR scan, several million target points are collected and processed into an ultra-high resolution terrain model of the damaged ground or structure. Scanning time for each tripod setup is extremely rapid, typically less than 5 minutes, and high accuracy geo-referencing of the damaged terrain imagery is accomplished through real-time dual-band Differential Global Positioning Satellite (DGPS) positioning. Post-processing of the point-data results in a triangular networked surface from which topographic change, deformation, and failure mode can be analyzed and visualized. In this paper, we present several examples of damage-visualization using ground-based LIDAR from the 2004 Niigata Chuetsu Earthquake (M6.6).

INTRODUCTION

A Tripod LIDAR system was deployed by the Earthquake Engineering Research Institute (EERI) to the central-Niigata Prefecture, Japan area the week following the

October 23, 2004, magnitude 6.6 earthquake, to evaluate the system as an earthquake response tool. The intent of the LIDAR deployment was to (1) assess the ability of the technology to image ground and structural deformations; (2) develop three-dimensional imagery of surface deformation, and (3) establish an ultra-high precision baseline survey for future change detection. We determined that the Tripod LIDAR system can resolve and map surface features that are a few centimeters in size, and precisely characterize the highly complex surfaces of large areas. In recent studies of the 2004 Parkfield Earthquake (Bawden, et al. 2004) and Denali Fault 2002 earthquake (Kayen et al., 2004a, 2004b), LiDAR technology was successfully used to image centimeter-scale data-sets for fault scarp morphology and after-slip change detection.

METHODS OF LIDAR ACQUISITION

The technology of 3-D scanning lasers is a natural extension of laser range finder systems used commonly in survey applications. With this technology, the laser rotates to acquire an angular-cylinder of point measurements (point cloud data) at a very rapid rate. As the rotating laser targets objects of varied distance from the scanner, point measurements are collected as well as natural color and reflectance intensity. The 3D laser scanner calculates the distance to an object based on the two-way travel time of the light pulse reflected off the objects surface. In this paper we discuss the application of 3-D laser scanning to deformed ground and structures affected by an earthquake, though the detailed measurement of complex topography can be made on any natural or man-made solid object (Collins and Sitar, 2004; Niemi et al, 2004).

The USGS scanning device used in Niigata was a Riegl z210i 3D-laser, a near-infrared imaging sensor. This device is a rugged, portable sensor designed for the rapid acquisition of high-resolution three-dimensional imagery under outdoor conditions. A single laser scan sweeps through a 336°-horizontal rotation, targeting an 80°-wide vertical field-of-view during rotation. The negative space, where no information is gathered (in each individual scan) is a 24° wedge in the rotational plane of the scanner, and two 100° cones centered in the axis of rotation, above and below the sensor. We fill in these no-data holes by changing the orientation of the scanner, re-scanning, and merging (registering) two or more data sets. The acceptable distance range of targets is approximately 2m-400m (Figure 1) and at these distances the point measurement accuracy is 0.8-2.5 cm, depending on scanner and software settings. Time required for scanning the highest density of points per set up (5.6 million targeted points) is 11 minutes. Coarser point measurement, in the hundreds of thousands, takes less than 1 minute. At the highest resolution, the angular separation of the vertical line scans is 0.01°. Thus, the near-field point separation is less than 1 mm and the separation of the farthest data can be over 7 cm. At the longest target distances, atmospheric refraction can induce a minor, though detectable error in the distance and range.

The angular position of the laser-pulse leaving the scanner is controlled by precise stepper-motors within the unit. The scanner makes millions of individual x, y, z position measurements, at a rate of 8,000 points/second. These individual points, together, form a “point cloud” of data. Some scanners, including ours, also have either optical sensors or digital line-scan cameras that record reflective color and intensity. With the

addition of either a color channel or a digital image, the natural appearance of the surface can be draped on the three-dimensional (3-D) surface model. Several useful applications of the color and intensity channels are to extract non-topographic textural information about the target; identify color-based lithologic changes in the target; and enhance and identify geo-referencing reflectors that send back the strong reflected signal (Kayen et al., 2004).

To image a surface, the scanner is transported to the site in a travel-bag or backpack. The unit weighs 13 kg, and the accessory cables, tripod, battery and laptop can double the weight. We place the scanner on a tripod in front of the object of interest and connect the device to a battery and laptop computer for data storage and visualization. Typically, the scanner is set up upright with the unit rotating horizontally, though to image objects overhead or below, the scanner can be mounted sideways. For example, the scan of the Juestsu railway tunnel-portal failure at Kita-Horinouchi (discussed later in Figure 5) included sideways scans of the tunnel roof.



Figure 1. The USGS LIDAR unit, here, scanning of a road embankment failure on Route 252, west of Horinouchi-Cho. The system can be easily transported by vehicle or backpack to study sites, and travels as checked baggage.

The 3-D laser scanners cannot see behind objects, and so the first surface encountered casts a shadow over objects behind it. For example, in a scan of the boulder-field of the White Rock Landslide at Ojiya, Japan (Figure 2), the near-field objects cast shadows over the debris located behind them. As the grazing-angle of the laser point decreases, proportionally larger shadows are cast on the ground behind the target. To minimize shadow zones and get full coverage of the target surface, the scanner is

moved to typically, three or more locations surrounding the target zone. Multiple setups limit the number of shadow zones while also increasing the resolution of the data collected and the outermost boundaries of the scanned area.



Figure 2. The landslide at White Rock, Ojiya swept portions of the highway, bluff, and vehicles into the Shinano River. Here, on the south side of the slide, the landslide buried the highway.

DATA HANDLEING IN LIDAR IMAGERY

A typical scan data set consists of many millions of data points. Efficient manipulation of that data is best performed on computers with the highest currently available processing speed, maximized dynamic RAM memory, and a video card with a large 128MB or 256MB memory buffer. Also, the manipulation of so many points requires specialized surface modeling software. Most laser manufacturers either distribute or suggest a specialized software program that is coupled with the laser. Our system utilizes a surface modeling software package called I-SiTE 3D (I-SiTE Inc., 2004) that collects both the scan point-cloud data and can process multiple scans into geo-referenced surfaces. After data is acquired, we typically follow a suite of standard processing steps to produce a surface model. First, the multiple scans are either locally or absolutely georeferenced to one-another. A least squares “best-fit” match is made between scans, augmented by precise survey measurements made with a total station or differential global positioning satellite (e.g., real time kinematic RTK-GPS, or Omnistar HP-differential GPS). Filters are then used to eliminate unwanted data. For example, we typically apply filters to remove vegetation so as to observe the bare earth. The

filtered point-data is our working digital terrain model (DTM) used to render a surface of the object (e.g. the topographic ground surface). Again, different surface modeling schemes can be used to render a surface from multiple scans. We can fuse multiple processed surfaces into a new composite surface for yet large more complex models. The surface model can be used to document the condition of the ground and provide a baseline for change detection of volumes, areas, and distances.

LIDAR IMAGERY FROM THE 23 OCTOBER 2004 NIIGATA CHUETSU, JAPAN (M6.6) EARTHQUAKE

During our reconnaissance of the 23 October 2004 Niigata Chuetsu, Japan earthquake, we visited sites of damaged roadways, structures, and displaced ground and collected data from approximately thirty individual laser-scan setups. The Niigata Chuetsu earthquake was particularly damaging to the roadways and hill-slopes in the mountain country above the Shinano and Uono rivers. Roadside embankment failures were ubiquitous throughout the mountainous areas. An example of one such embankment failure on a steep mountainous section of Highway 252, west of Horinouchi Town is presented in Figure 1 and 3.

Here, a two-way, two-lane road, built on the northern side of a steeply sloped river-incised canyon, failed toward the south into the bottom of a narrow ravine. Two scans were set up on the east and west ends of the failure to minimize the shadow zones. In the four frames of Figure 3, we show the processing procedures for producing a surface model: (A) scan the target from multiple perspectives; (B) merge and register the scans; (C) filter out vegetation and render the surface model; and (D) visualize and analyze surface model with overlay of raw point data. With this product, we can make a variety of geometric measurements of the ground failure and have a data set that can be differenced against pre-event topographic survey drawings of the embankment.

An example of structural damage recorded by the LIDAR unit is presented in Figure 4, collected in the damaged portal of the Juetsu railroad tunnel, north of the town of Horinouchi in central Niigata prefecture. The portal is founded on a poorly compacted embankment fill that settled during the earthquake. The portal pulled away from the tunnel, opening a gap, and settled laterally toward the east (downslope). Vertical settlement was more pronounced on one side of the portal causing it to undergo a minor rotation. A photograph of embankment and tunnel damage is presented in Figure 4A. In the interior of the tunnel, displacement of the portal was observed in the walls and ceiling. An oblique view of the LIDAR point-cloud data can be seen on the right in Figure 4B. Here, the portal (front section) and tunnel are viewed from above and south of the portal entrance. The left-lateral offset of the portal relative to the tunnel is clearly visible in the LIDAR model. In the LIDAR imagery, precise centimeter-scale measurements can be made of the three-dimensional deformation of the structure. At this tunnel, we measure 36 cm of separation of the portal and 21 cm of left-lateral displacement. Displacement of the portal and failure of the gravel embankment also resulted in deformation of the railway tracks, clearly visible in the LIDAR scans.

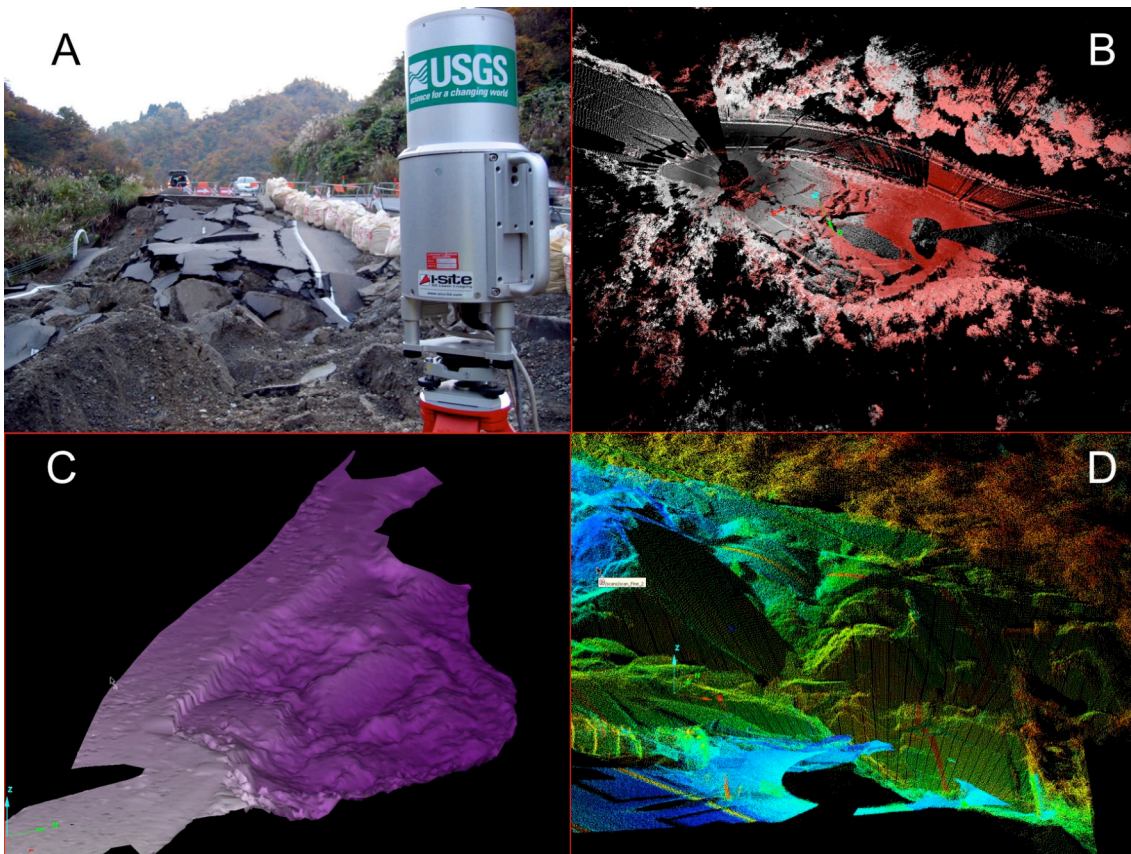


Figure 3. Processing procedures for ground-LIDAR technology: (A) scan target; (B) merge multiple scans; (C) render the solid surface model; (D) visualize and analyze geometry. The direction arrows are the local orientation of the scanner and not the absolute orientation.

We use 3-D imaging software to rotate the LIDAR imagery into plan view looking down from above through the roof of the portal (Figure 5). In this view, the portal separation (35 cm) and left-lateral displacement (21 cm) from the tunnel (right) can be seen at the top and bottom of the tunnel wall. The data-hole in the center is the non-illuminated area beneath the tripod.

A final example is of a natural slope failure is the White Rock landslide, which dislodged rock debris along a steep un-buttressed cliff corner on the banks of the Shinano River, at Route 17. This huge rockslide at Myoken, Ojiya-Shi, dislodged a n entire cliff-face of soft and friable weathered mud stone with laminated sand. This slide killed several people driving along on the National Road 17 along the Shinano River. The rock slope, a portion of the highway cut-and-fill, and five vehicles were swept into the Shinano River in a catastrophic collapse of the bluff. Eight LIDAR scans were taken on the north, western and southern sides of the slide to characterize the volume, runout and morphology of the slide. The roadbed on the north side of the slide collapsed into the river. On the south side of the landslide, block debris completely covered the roadbed just north of the highway bridge (Figure 2). The height of the cliff

at Shirowa is on average meters and the run out distance is 130 meters, on average. The road bed at the southern end of Route 17, just north of the bridge was completely covered with debris. That road bed was 13 meters above the Shinano River toward the base of the slope, well down slope from the crest of the cliff that released the rock avalanche. Thus the impact of the falling rock on the road must have been devastating. A number of the largest intact boulders in the avalanche are in excess of 6 meters to a side.

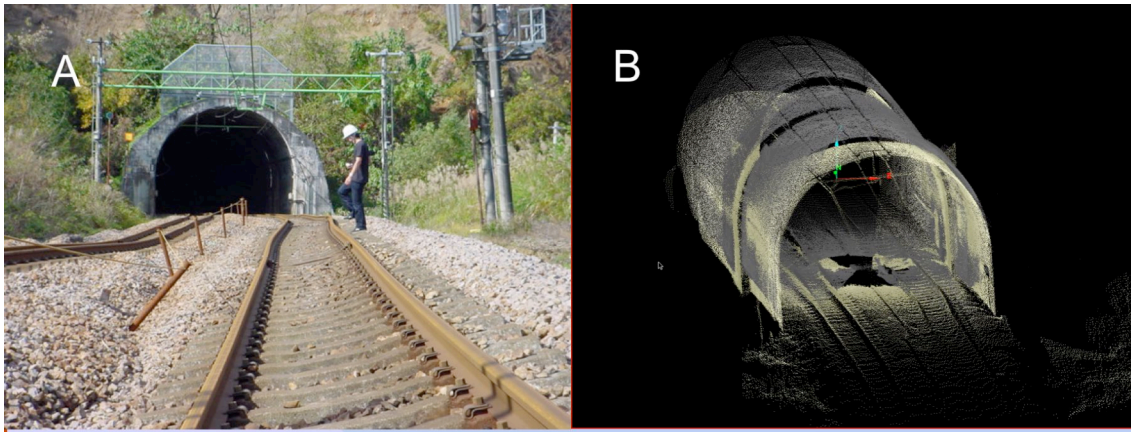


Figure 4. Photograph (A) and LIDAR image (B) of damage to the Juetsu Railroad portal at Kita-Horinouchi. Lateral displacement of the portal relative to the tunnel wall and distress of the rail track is precisely recorded in the LIDAR scan (B).

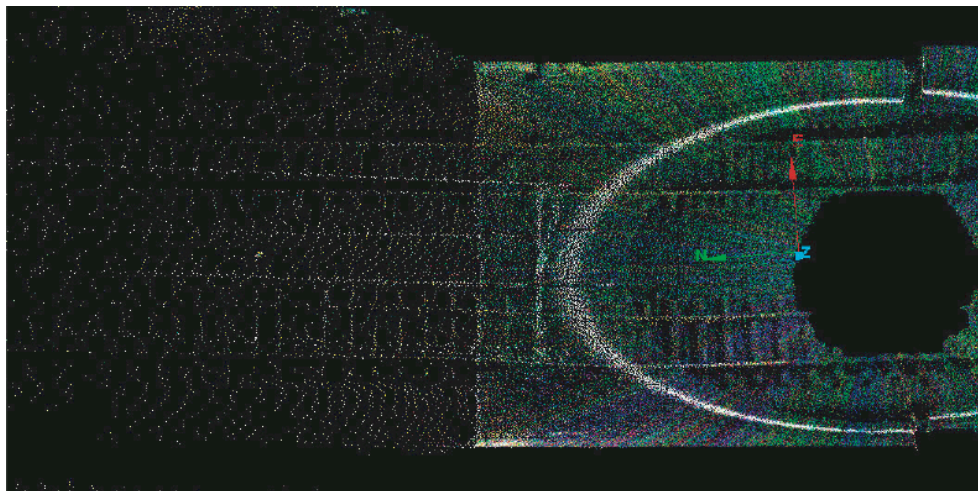


Figure 5. Plan view perspective of the LIDAR image of damage to the Juetsu Railroad portal at Kita-Horinouchi. Portal displacement is 21 cm lateral-toward the left. The direction arrows are the local orientations of the vertical and horizontal planes about the scanner and are not absolute directions.

SUMMARY

In this study, we used ground-based tripod-mounted LIDAR to map the complex topography of geotechnical and structural failures that occurred during the Niigata Ken Chuetsu earthquake. There are several benefits in acquiring these LIDAR data in the initial reconnaissance effort after the earthquake. First, we record the detailed failure morphologies of damaged ground and structures in order to make measurements that are either impractical or impossible by conventional survey means. The digital terrain models (DTM's) allow us to enlarge, enhance and rotate data in order to visualize damage in orientations and scales not previously possible. This ability to visualize damage allows us to better understand failure modes. Filtering techniques allow for the removal of vegetation, so that we can assess the deformations on the bare earth. Finally, LIDAR allows us to archive 3-D terrain models of damaged ground and structures so that the engineering community can evaluate analytical and numerical models of deformation potential against detailed field measurements. LIDAR has proven to be a useful addition to the various tools we bring to earthquake reconnaissance, and will likely be a standard component of future response efforts.

REFERENCES

- Bawden, G.W., Kayen, R., Silver, M.H., Brandt, J.T., Collins, B.D. (2004) Evaluating Tripod Lidar as an earthquake response tool, *Eos Trans. AGU*, 85(47), Fall Meet. Suppl., Abstract S51C-0170R.
- Collins, B.D. and Sitar, N. (2004) Application of High Resolution 3D Laser Scanning to Slope Stability Studies, 39th Symposium on Engineering Geology and Geotechnical Engineering, Butte, Montana, 14 p.
- Kayen, R., Barnhardt, W., Carkin, B., Collins, B.D., Grossman, E.E., Minasian, D., Thompson, E. (2004) Imaging the M7.9 Denali Fault Earthquake 2002 rupture at the Delta River using LiDAR, RADAR, and SASW Surface Wave Geophysics, *Eos Trans. AGU*, 85(47), Fall Meet. Suppl., Abstract S11A-0999.
- Niemi, T.M., Kayen, R., Zhang, H., Dunn, C.R., Doolin, D.M. (2004) LiDAR Imagery of the San Andreas Fault Zone at the Vedanta and Olema Ridge Paleoseismic Trench Sites, Pt. Reyes, CA, *Eos Trans. AGU*, 85(47), Fall Meet. Suppl., Abstract G13B-0811.